AMES GRANT
IN-02-CR
115289
32P

FIRST SEMI-ANNUAL STATUS REPORT
NASA RESEARCH GRANT NO. NAG. 2-462

For Period Covering 1 July 1987 to 31 December 1987

DEVELOPMENT OF AN UNSTEADY WAKE THEORY APPROPRIATE FOR AEROELASTIC ANALYSES OF ROTORS IN HOVER AND FORWARD FLIGHT

by

David A. Peters
Principal Investigator
School of Aerospace Engineering
Georgia Institute of Technology
Atlanta, Georgia 30332-0150

January 4, 1988

Background

The purpose of this research is the development of an unsteady aerodynamic model for rotors such that it can be used in conventional aeroelastic analyses (e.g., eigenvalue determination and control-system design). For this to happen, the model must be in a state-space formulation such that the states of the flow can be defined, calculated, and identified as part of the analysis. The proposal upon which this work is based presented such a state-space model. In that model, the induced flow is represented as an expansion both radially and azimuthally. Although, in principal, any expansion functions could be used, there is computational advantage in using Fourier components in the azimuthal direction and either Legendre functions ($P_n^m(\nu)$ where $\nu = \sqrt{1-r^2}$) or $P_n^m(\nu)/\nu$ in the radial direction.

The fluid mechanics of the problem is given by a closed-form inversion of an acceleration potential. The result is a set of first-order differential equations in time for the unknown flow coefficients. These equations are hierarchical in the sense that they may be truncated at any number of radial or azimuthal terms. It should be noted that we have consistently underestimated the richness and rigor of this approach and have been surprised several times by what effects are implicitly included in such a model. The coefficients of the first-order equations can be written explicitly in terms of certain integrals of the Legendre functions taken over the disk or along streamlines. The right-hand-side of the equations are written in terms of integrals of the blade loading which must come from a blade lift theory such as 2-D quasi-steady theory, dynamic stall models, or any other lift methodology.

Although the theory is, in principal, "written down", much remains to be done before it can be a viable theory for use by designers and researchers. First, all of the coefficient matrices need to be determined either numerically or (whenever possible) in closed form for easy application. Second, the convergence properties of the method must be studied to determine how many shape functions are required to match a particular phenomenon. Third, theoretical studies need to be performed to determine the strengths and

limitations of the model. We already know that the model implicitly includes:

1.) The near-wake approximation to the Theodorsen Function
2.) Loewy Theory (with improved time constants) in hover
3.) Dynamic Inflow Theory
4.) Hover momentum theory with implicit account of tip losses
5.) Bessel Function behavior of lift with reduced frequency
6.) Unsteady flow anywhere in the flow field

However, we do not know how many terms are required to capture these effects to a given accuracy; and we do not know the best scheme for distinguishing between induced flow due to bound vorticity and flow due to shed vorticity. These are the types of questions we expect to answer in this research.

Technical Personnel

Three people have been supported on this grant during the first six-month period. The principal investigator, David A. Peters, has contributed 1.0 man-months; a full-time graduate assistant, Cheng-Jian He, has contributed 2.0 man-months; and another graduate student, Ay Su, has contributed 1.0 man-months. Both of these students are working toward Ph.D. degrees. A third student, David Doug Boyd, is working on the project but is being supported by Georgia Tech funding. He is working toward a Master of Science Degree in Aerospace Engineering.

Radial Convergence Issues

In order to adequately address the convergence issues, we have assembled a dynamic set of equations for rigid or elastic blade flapping in hover including the wake state variables. Mr. Su is in charge of this work. We are presently exercising this model in hover to determine these convergence properties. We must first concentrate on hover both because it is the more fundamental regime and because the forward flight model is still under development. The first area we addressed was convergence to the quasi-steady

lift-deficiency function of Sissingh, Curtiss, and Shupe. For this to occur, a certain matrix inner product ($Q=Z^T B^{-1} Z$) must converge to 15/8 = 1.875 (where only the zeroeth harmonic is required).

Figure 1a shows the convergence of Q when the shape functions are the Legendre Functions. For this case, B=I; and Q reduces to $Z^T Z$. For only one shape function, there is 25% error; but this error is reduced to 2% for two functions and to essentially zero for four functions. Figures 1b and 1c show the same plot when $P_n^m(\nu)/\nu$ are taken as the shape functions. In that case, $B=\bar{B}=\bar{A}^{-1}$, both of which are known in closed form. However, $\bar{B}$ is only equal to $\bar{A}$-inverse in the limit as the number of functions goes to infinity. Therefore, we have the option of using the truncated $\bar{A}$ matrix (Fig. 1b) or of inverting the truncated $\bar{B}$ matrix (Fig. 1c). In the former case, one shape function gives the exact answer; but two shape functions increases the error to 12%. This fortunate occurrence at S=1 explains why dynamic inflow (with only one shape function) can give the exact lift deficiency. On the other hand, though, the use of a truncated $\bar{A}$ matrix gives poor convergence as S increases. The inverse of the truncated $\bar{B}$ matrix (which is what one would obtain in a straightforward application of the theory) has a 12% error at S=1, but it converges very rapidly to the exact answer. (This 12% error is exactly the 8/9 discrepancy between Sissingh and Shupe due to assumption on inflow distribution.) Therefore, based on quasi-steady inflow, one would predict that a conventional application of $P_n^m(\nu)/\nu$ is the best choice of shape function.

The next step in this area has been to see how these conclusions vary when unsteady terms are added. In this part of our research, we consider full coupling between all harmonics and the blade. This results in equations with periodic coefficients (even in hover). In earlier work, we saw these periodic coefficients and thought there was an inconsistency. Actually, there is no inconsistency. The periodic coefficients describe the true rotating to nonrotating coupling of rotor and wake. When multiblade coordinates are used for the rotor, most of the periodic coefficients vanish; but some remain if more inflow harmonics exist than there are blades. In the results of Figs. 2 and 3, we neglect periodic coefficients. This is equivalent to study of only the collective flapping mode with collective inflow.

This allows us to view the unsteady effect in a simple setting. However, by keeping the uncoupled harmonics in the analysis (M=2), we can also compare the uncoupled inflow time constants with known, closed-form solutions.

Figures 2 and 3 show the effect of shape functions (and, thus of the inflow dynamics) on the rigid flap damping, collective mode. Figures 2a and 2b give the Real and Imaginary parts of the fundamental eigenvalue for $P_n^m(\nu)$ as the shape functions. With no dynamic inflow, the Real portion is $-\gamma/8 = -.325$; but, as shape functions are added, the solution approaches -.2925. The quasi-steady value is -.2167, but the time lag has lessened the lift deficiency. Interestingly, it takes 2 shape functions to converge to within 3% and four shape function to converge completely. Figures 3a and 3b provide a similar plot but with $P_n^m(\nu)/\nu$ as the shape functions. Here, a similar convergence pattern appears.

The future direction of our work in this area is the inclusion of complete, periodic-coefficient coupling. We intend to study the interaction of various Floquet modes with the inflow. Hopefully, this will illuminate the effects of all types of rotor modes (collective, cyclic, differential, etc.) even though we have only a one-bladed model. However, we are prepared to add more blades if that is necessary.

The last area of radial convergence has to do with tip loss. Figures 4a and 4b provide static inflow distributions from our theory (unsteady terms set to zero) for $\Theta=1$. Figure 4a is with $P_n^m(\nu)/\nu$ and Fig. 4b is with $P_n^m(\nu)$ for the shape functions. First, we examine Fig. 4a. The dashed-dot line is the solution with no tip loss. The solution well approximates the straight-line with slope of 1/3 which is the exact solution for inflow. The dashed line is the solution when Prandtl's tip-loss function is applied to the right-hand side of the equations; and the solid line is the exact Prandtl solution. It takes about 8 shape functions to fit this behavior, although many fewer give the correct tip-loss factor. In contrast, we see that the Legendre functions $P_n^m(\nu)$ do a poor job of matching quasi-steady values, Fig. 4b. Although the functions "do their best" to fit the true behavior, the fact that they are zero at r=1 precludes any true convergence. Based on these results, we abandoned $P_n^m(\nu)$ and are continuing only with $P_n^m(\nu)/\nu$.

Harmonic Convergence

A second important area of our research has been in harmonic convergence, and part of the results were unexpected. In particular, we were surprised in the area of tip-loss factor. As background, recall that our original work on this method suggested using Prandtl's tip-loss function on the right-hand-side of the equations in order to force the lift to zero (and the inflow to be finite) at the tip. We wanted to do this because, in quasi-steady inflow theory, the induced flow must follow the pressure distribution. Thus, the lift does not drop off at the tip. What we failed to recognize, however, was that quasi-steady theory is equivalent to an infinite number of blades for which there is no tip loss. When we add the unsteady terms, this changes. For example, in hover (even for constant collective pitch) the wake sees a periodic pressure excitation due to blade passage. Although the fundamental (zero) inflow harmonic will exactly match the shape of the pressure distribution, the higher harmonics are influence by the unsteady operator which gives inflow that varies as $1/\sqrt{1-r^2}$ near the tip. This forces large induced flow at the tip which decreases lift.

Figure 5a shows this effect for S=1. The results are inflow distributions with no tip-loss "correction" but with the unsteady, blade-passage terms included. One sees how the inflow begins to climb near the tip as more and more harmonics are added. Figure 5b shows the effect as more radial functions are added at M=4. By S=4, the solution has essentially converged to the Prandtl tip-loss function (compare Fig. 4a). It is also interesting that fewer shape functions are required to capture tip losses in this unsteady manner than were necessary in the quasi-steady version with a correction. The reason for this is that the higher-harmonic shape functions (m larger) automatically are weighted toward the tip region as m increases. Thus, fewer are needed to match the rapid tip-loss gradients near the tip. It is also interesting that the true tip-loss behavior has come forth from an unsteady term, although tip loss is thought of as a static phenomenon. Remember, however, that the "unsteady" harmonic inflow terms (as seen in the nonrotating system) can be viewed as static with respect to a moving blade. This result adds another impressive item to the list of important effects that are automatically included in our unsteady theory.

A final area of questions on harmonic convergence deals with the convergence of induced flow near the blade and the effect of the bound vorticity. In our earlier work, we found that induced flow at some points could slowly diverge due to the effects of bound vorticity on the blade. Usually, not enough harmonics are retained to make this a practical problem (the truncation filters the spike near the blade). However, we know that we must study this phenomenon for several blade chord-wise loadings to determine the true effect. This is the work of Doug Boyd. He has completed the debugging of his computer program, and we are only now beginning to interpret the results. However, we expect some important answers soon.

Closed-Form Results

Another important area of our research is the development of closed-form expressions for the matrices and influence coefficients of our theory. This is necessary not only for the pursuit of our research but also so that others will be able to use the model with ease. Mr. Cheng-Jian He is the lead research assistant in this area.

Table 1 provides a summary of the important relations that we have developed. None of these have we seen in the literature (save for the ρ_n^m integral). They have been derived by a combination of good fortune and clever manipulations. For example, we originally had closed-form results for the first row-column of each $\bar{A}$ matrix ($l=m+1$) and for the diagonals of the $m=0$ $\bar{A}$ matrix. From this, we guessed a form for a general A and it agreed with numerical results for as many decimals as we could calculate for all (m,l,n) combinations. From this and the Legendre recursion formula, we were able to find $\bar{I}_n^m$; and, from that, we developed the B_n^m formula. Then, a comparison of $\bar{I}_n^m$ and ρ_n^m and a known result for $m=0$ gave the general $P_n^m P_l^m$.

The existence of general $\bar{A}$ and $\bar{B}$ matrices implies that the hover theory can now be applied in complete generality without the need for numerical integrals on the left-hand side. This also implies that we are able to obtain the eigenvalues and modes of the inflow model. These come from the matrix $[K_n^m]^{1/2}[A][K_n^m]^{1/2}$. Interestingly, this matrix comes in closed form

(Table 1) and is independent of explicit m dependence! However, the eigenvalues do depend on the value of m because one takes only the m+1, m+3, m+5, ... rows and columns for the mth harmonic. The modes follow expected oscillatory patterns in r with more oscillations as n increases for any m. Figure 6a shows these modes for the fundamental eigenvalue (m=0,4), and Fig. shows the second mode for each harmonic. What is interesting is that the modes all have zero flow at the blade tip which means that either of our candidate shape functions would converge. The zero-velocity condition at the tip occurs despite the fact that the forced inflow response does not exhibit this boundary behavior.

The eigenvalues, which are the time constants of the flow, follow definite patterns in the root locus plane. Although they are purely real, they tend to couple with modes (in the rotating system) that have frequencies close to m. Thus, we can predict which modes might be affected by each inflow state variable. Table II lists the fundamental time constant for each harmonic and compares it with both the geometric mean approximation (used in our previous work) and the Pitt model. We note that the fundamental time constants are close to the geometric mean approximation, which is indicative of the fact that they are dominated by the lowest order Legendre function. We also not that the Pitt model underestimates the time constants of higher modes.

The final area to be discussed is the development of the LL_{ln}^{rm} matrix which contains the influence coefficients between all harmonics and all shape functions. Recall that this matrix depends only on wake skew angle. The computation of this matrix is a monumental task both because of the complexity of the Legendre functions (which are integrated along streamlines to infinity) and because of the number of terms. For example, for 8 harmonics and 6 radial functions per harmonic, we would have $[(8+1)*(6)]^2+[(8)*(6)]^2$ = 5,220 terms, each a function of the skew angle β. This is too much information to pass to every potential user. It now appears, however, that we will be able to condense the model down to only a few crucial numbers. Presently, we have computed numerical values for 4 harmonics and 3 shape function at values β=0°, 30°, 60°, and 90°. Based on this, we have determined that each mr combination is governed by a simple function of $\tan(\beta/2)$ independent of n

and 1. We now have these functions in closed form for both the cosine and sine LL matrices. Now, we are working on a simplified form for the coefficients themselves.

To do this, we will need to calculate coefficients for higher harmonics. However, this becomes increasingly difficult as the sum of m+n increases. Thus, we are working on more efficient means of generation of Legendre functions. We hope, ultimately, to have a short Legendre Function subroutine that potential users could copy in order to use these functions in their own modal integrals. Needless to say, we are very excited about these developments for the LL matrices and look forward to completion of that part of the work. Once the LL matrices are known, we can begin to study the convergence of our method in forward flight and see how it might affect flap dynamics.

Summary

Our research is progressing very well in every way. We have been consistently surprised at the richness of physical description that is implicit in our model and at the simplicity of structure that falls out of seemingly hopeless complexity. We are right "on track" to complete all of our first-year goals and to begin the second-year effort in July. Sometime before then we would like to visit Ames, both to present more details about our findings and to answer any questions that the Army and NASA technical people might have.

Table I. Important Relations

$n+m$ odd, $\ell+m$ odd, $q+m$ even unless otherwise noted

$$\bar{P}_n^m(x) = P_n^m(x)/\rho_n^m \qquad \bar{Q}_n^m(i\eta) = Q_n^m(i2)/Q_n^m(i0)$$

$$(\rho_n^m)^2 = \int_0^1 P_n^m P_n^m \, dx = \frac{(n+m)!!\,(n+m-1)!!}{(n-m-1)!!\,(n-m)!!} \frac{1}{2n+1} \begin{cases} n+m \text{ odd} \\ n+m \text{ even} \end{cases}$$

$$K_n^m = \frac{-Q_n^m(i0)}{i\,Q_n^{m\prime}(i0)} = \underbrace{\left|\frac{2}{\pi}\right|}_{n+m \text{ odd only}} \frac{(n+m-1)!!\,(n-m-1)!!}{(n+m)!!\,(n-m)!!} \quad \left[\text{remove } \tfrac{2}{\pi} \text{ and use } \tfrac{\pi}{2} \text{ for } n+m \text{ even}\right]$$

$$\bar{I}_{nq}^m = \int_0^1 \bar{P}_n^m \bar{P}_q^m \, dx = \frac{1}{\rho_n^m \rho_q^m} \frac{(n+m)!!\,(q+m-1)!!}{(n-m-1)!!\,(q-m)!!} \frac{(-1)^{\frac{n+q-2m-1}{2}}}{(n+q+1)(n-q)}$$

$$\bar{A}_{n\ell}^m = \int_0^1 \bar{P}_n^m \bar{P}_\ell^m x \, dx = (K_n^m K_\ell^m)^{-\frac{1}{2}} \frac{2}{\pi} \frac{2\sqrt{2n+1}\sqrt{2\ell+1}}{(n+\ell+2)(n+\ell)} \frac{(-1)^{\frac{n+\ell-2m}{2}}}{\left[(n-\ell)^2-1\right]}$$

$$\bar{B}_{n\ell}^m = \int_0^1 \bar{P}_n^m \bar{P}_\ell^m \frac{1}{x} \, dx =$$

$$(K_\ell^m/K_n^m)^{1/2} \sqrt{2n+1}\sqrt{2\ell+1}\,(-1)^{\frac{n+\ell-2m-2}{2}} \sum_{\substack{q=m,\\ m+2,\\ m+4,}}^{\ell-1} K_q^m \frac{2q+1}{(n+q+1)(n-q)}$$

$$\int_0^1 P_\nu^m P_\lambda^m \, dx = 2^{2m}\left[\frac{Q^m(\nu,\lambda)\sin\left(\frac{\pi\nu}{2}\right)\cos\left(\frac{\pi\lambda}{2}\right) - Q^m(\lambda,\nu)\cos\left(\frac{\pi\nu}{2}\right)\sin\left(\frac{\pi\lambda}{2}\right)}{\frac{\pi}{2}(\nu-\lambda)(\nu+\lambda+1)}\right]$$

$$Q^m(\nu,\lambda) = \frac{\Gamma\left(\frac{\nu+m+2}{2}\right)\Gamma\left(\frac{\lambda+m+1}{2}\right)}{\Gamma\left(\frac{\nu-m+1}{2}\right)\Gamma\left(\frac{\lambda-m+2}{2}\right)} \qquad \text{general } \nu, \lambda, m$$

Table II. Time Constants of Fundamental Dynamic Inflow Modes

m	Eigenvalue	$t=0$ Geometric Mean	P.H
0	.4985	.4501	.4244
1	.2896	.2684	.2264
2	.2097	.1960	.1552
3	.1661	.1556	.1183
4	.1383	.1294	.0956

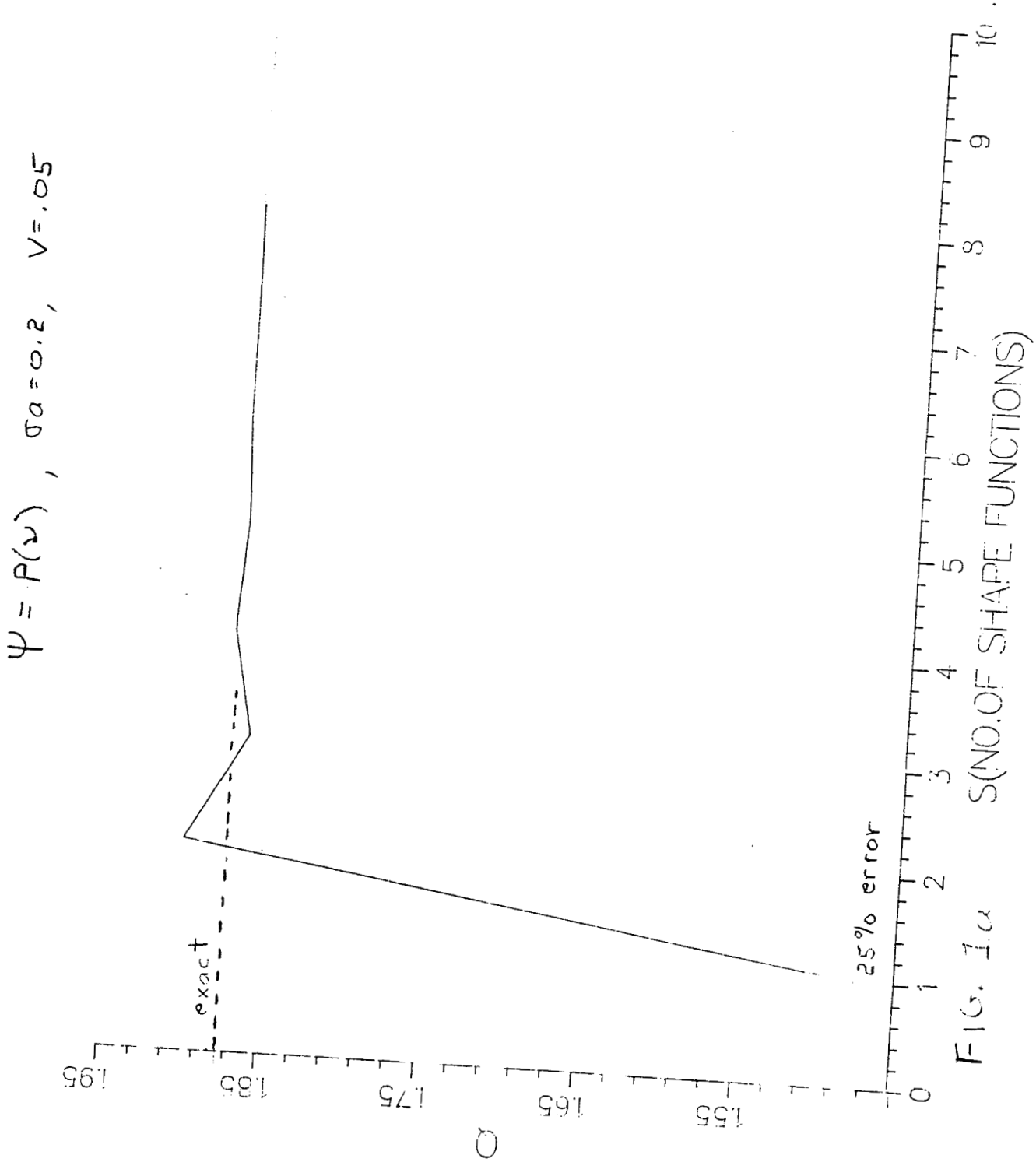

FIG. 1a

A--MATRIX(CLOSE FORM) $\psi = P(\nu)/\nu$

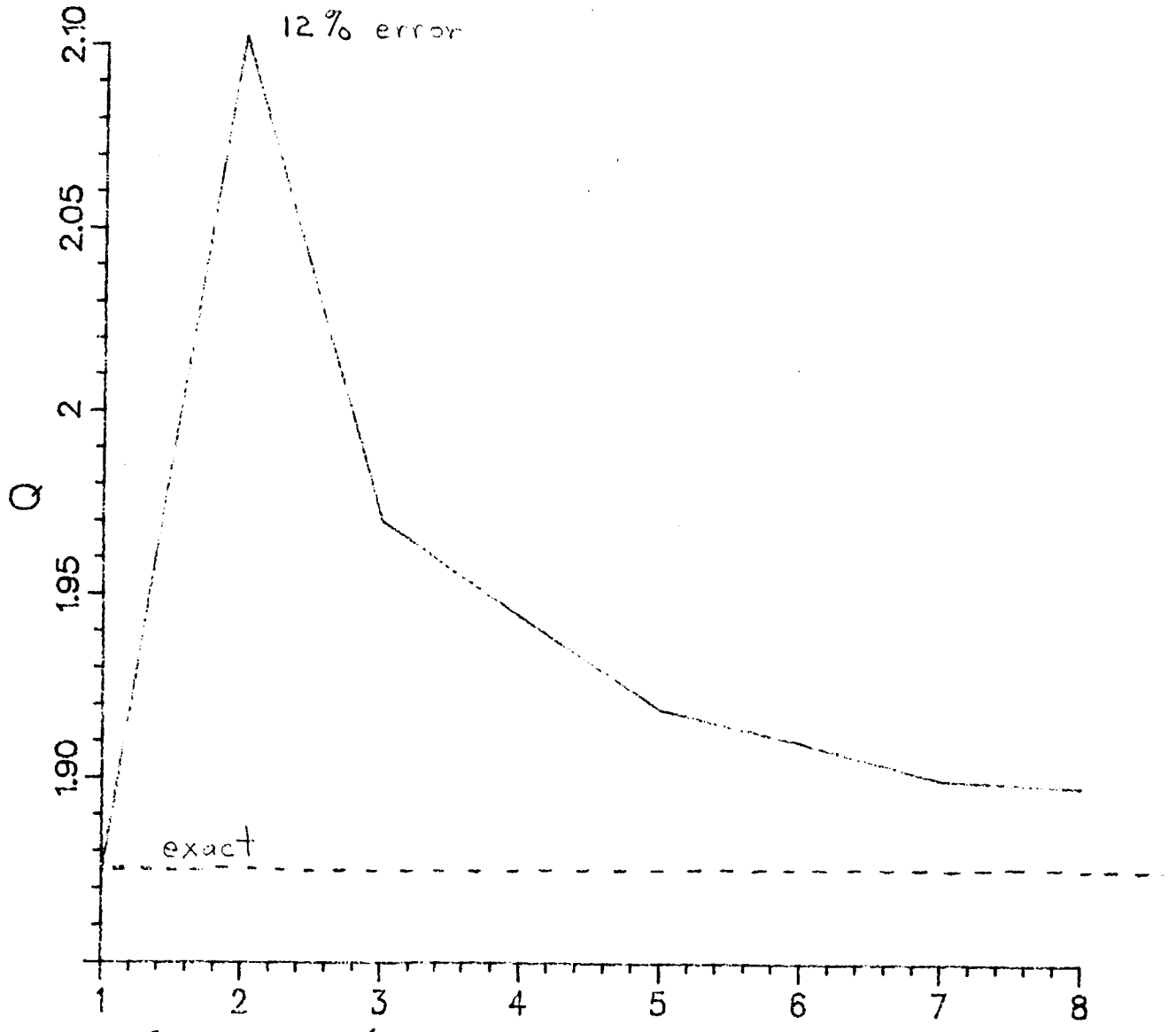

Fig. 1b

TRUNCATED B--MATRIX

$\psi = P(\nu)/\nu$

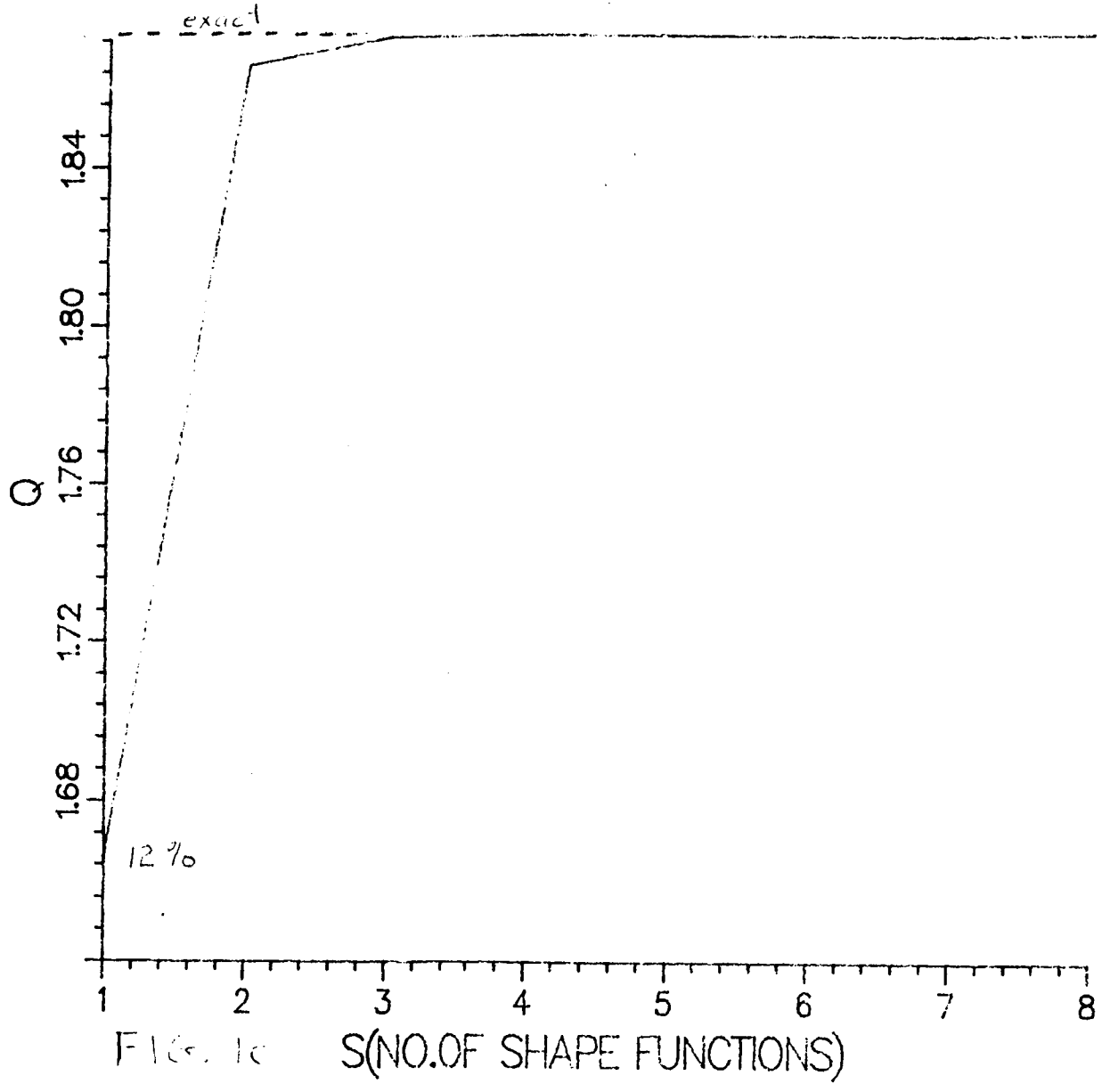

FIG. 1c

M–2, $\psi = P(2)$

$\gamma = 5$, $P = 1.15$

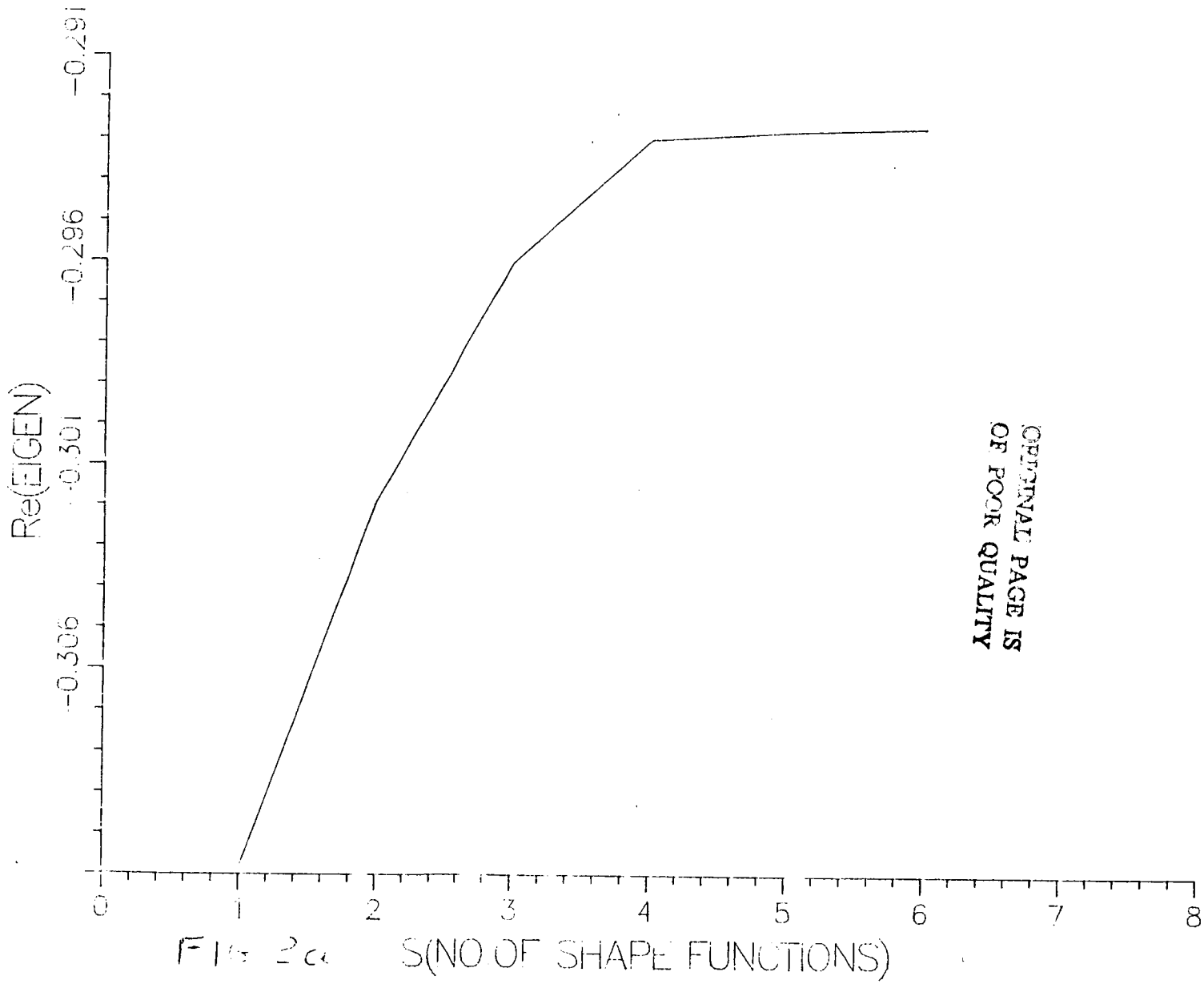

Fig. 2a

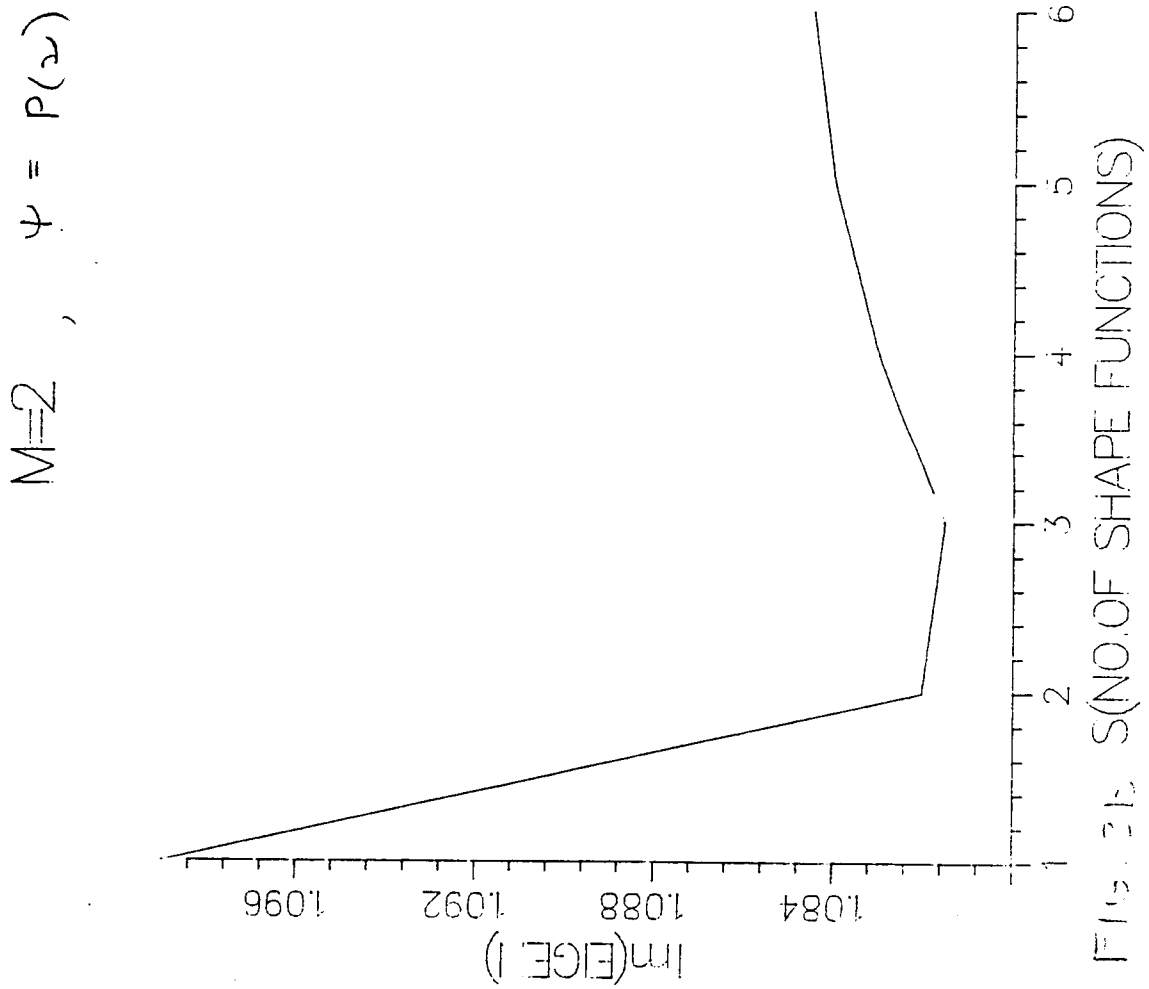

Fig. 21

M=2 $\Psi = P(\nu)/\nu$

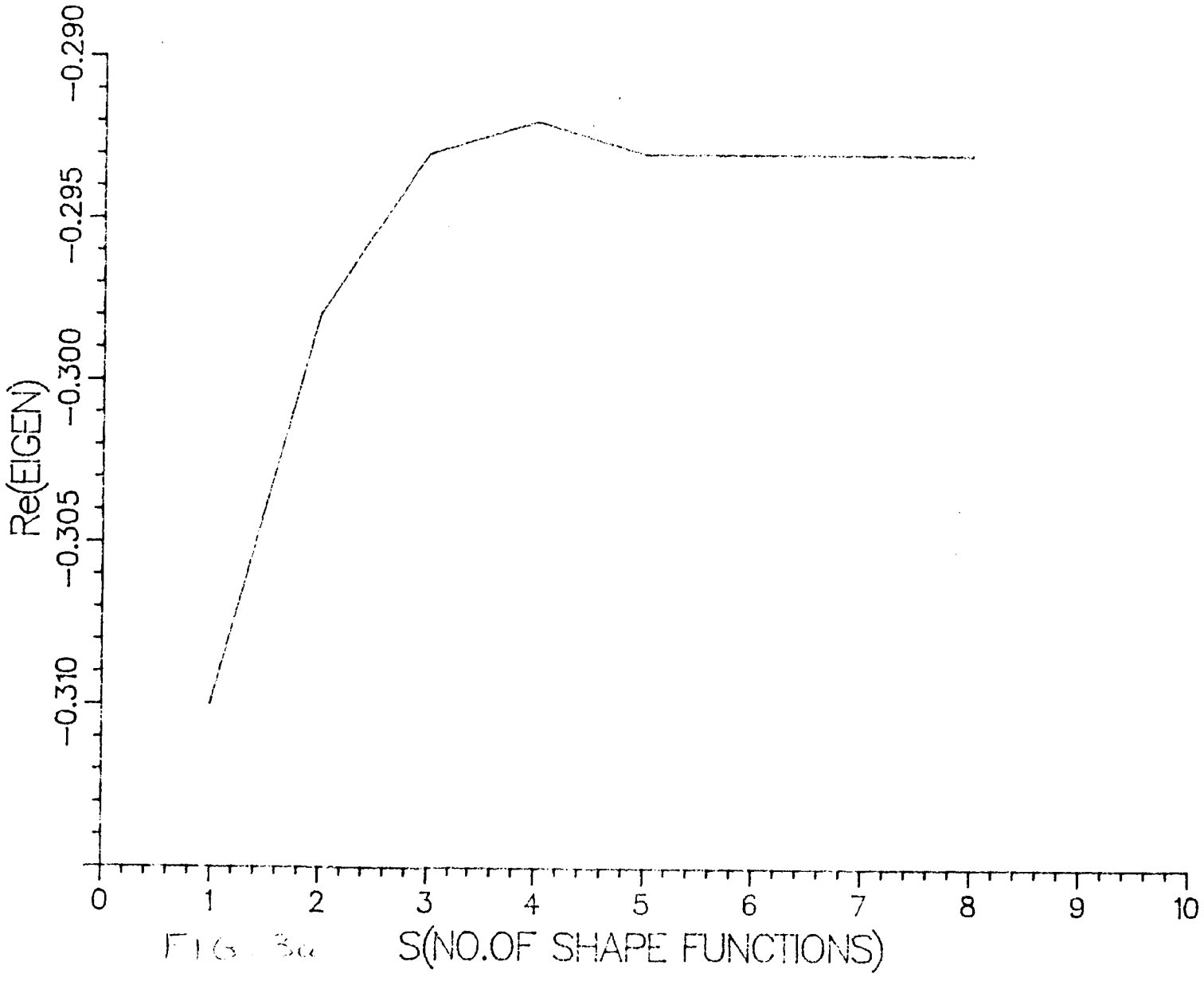

FIG. 3a

M=2 $\psi = P(\nu)/\nu$

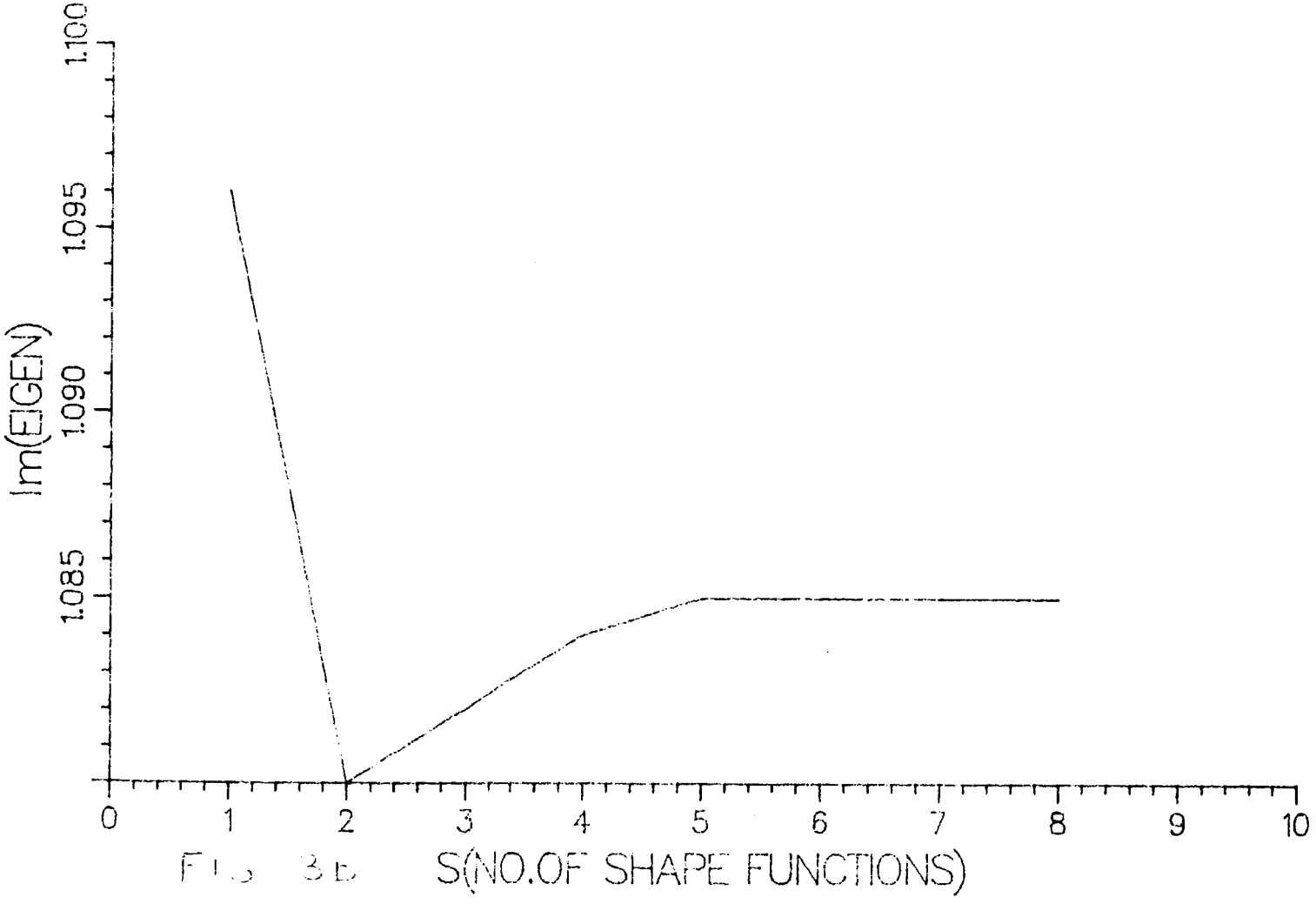

FIG. 3B

Fig. 4a S=8 CASE 1 ($\psi_s^m = \bar{p_e}^m / \nu$)

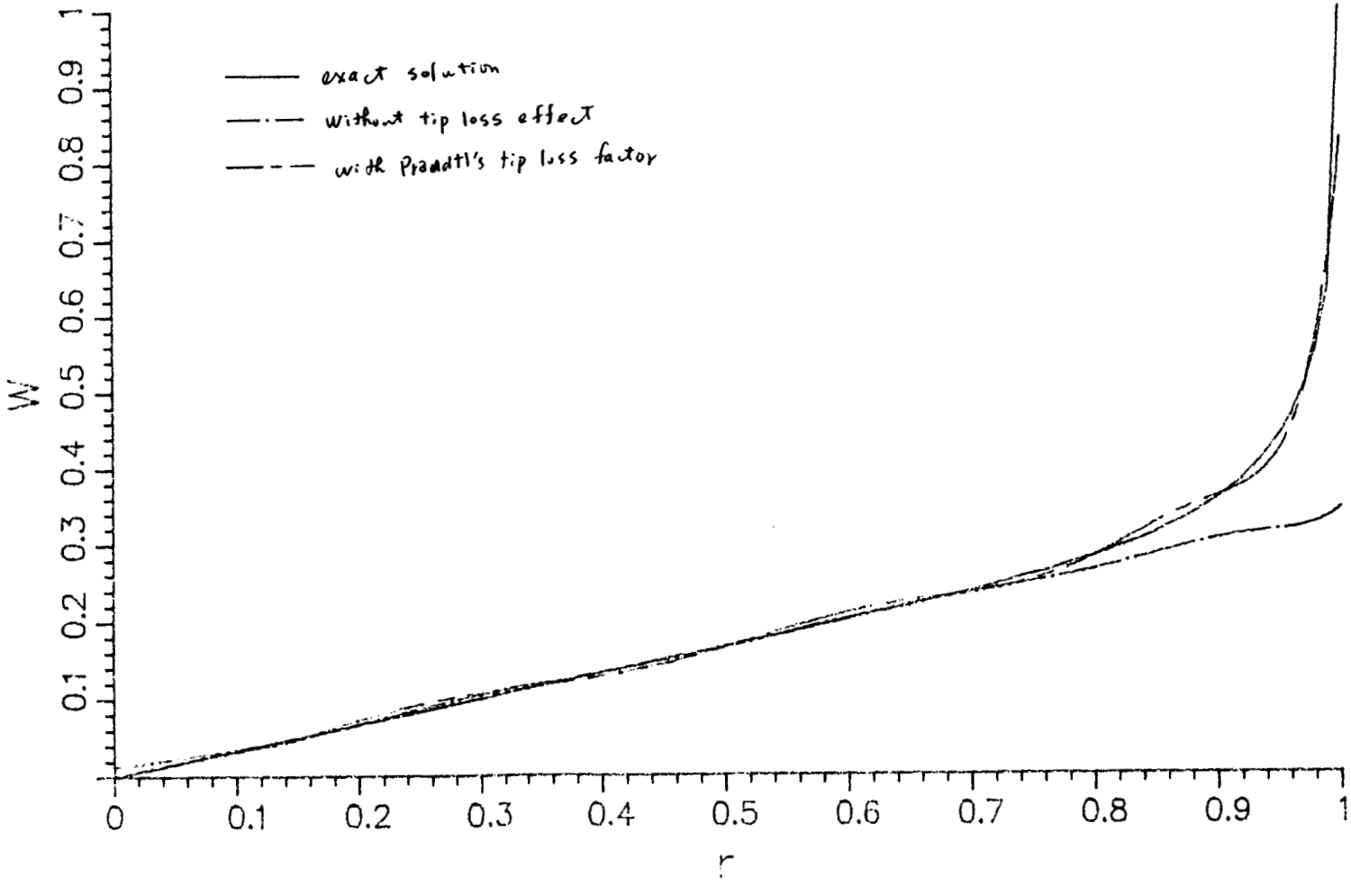

FIG. 4b S=8 CASE 2 ($\psi_s^m = \bar{P}e^m$)

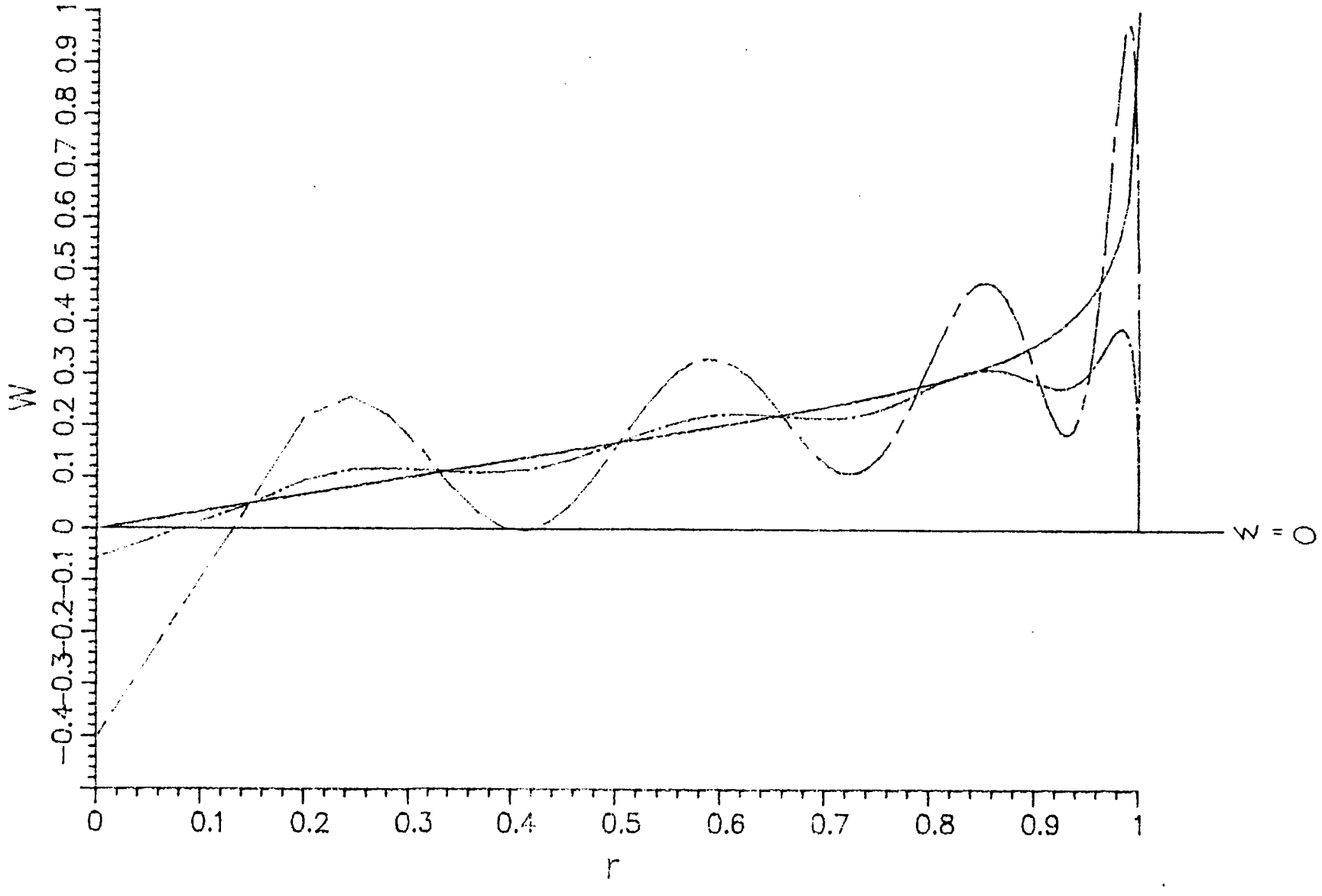

periodic coefficient

$\bar{p}_z^m/\nu = 4s^m$, $\beta = \beta^* = 0$, $a = 0.2$

$\theta = 1$

Fig. 5a EFFECT OF HARMONICS $s=1$ ON TIP LOSS

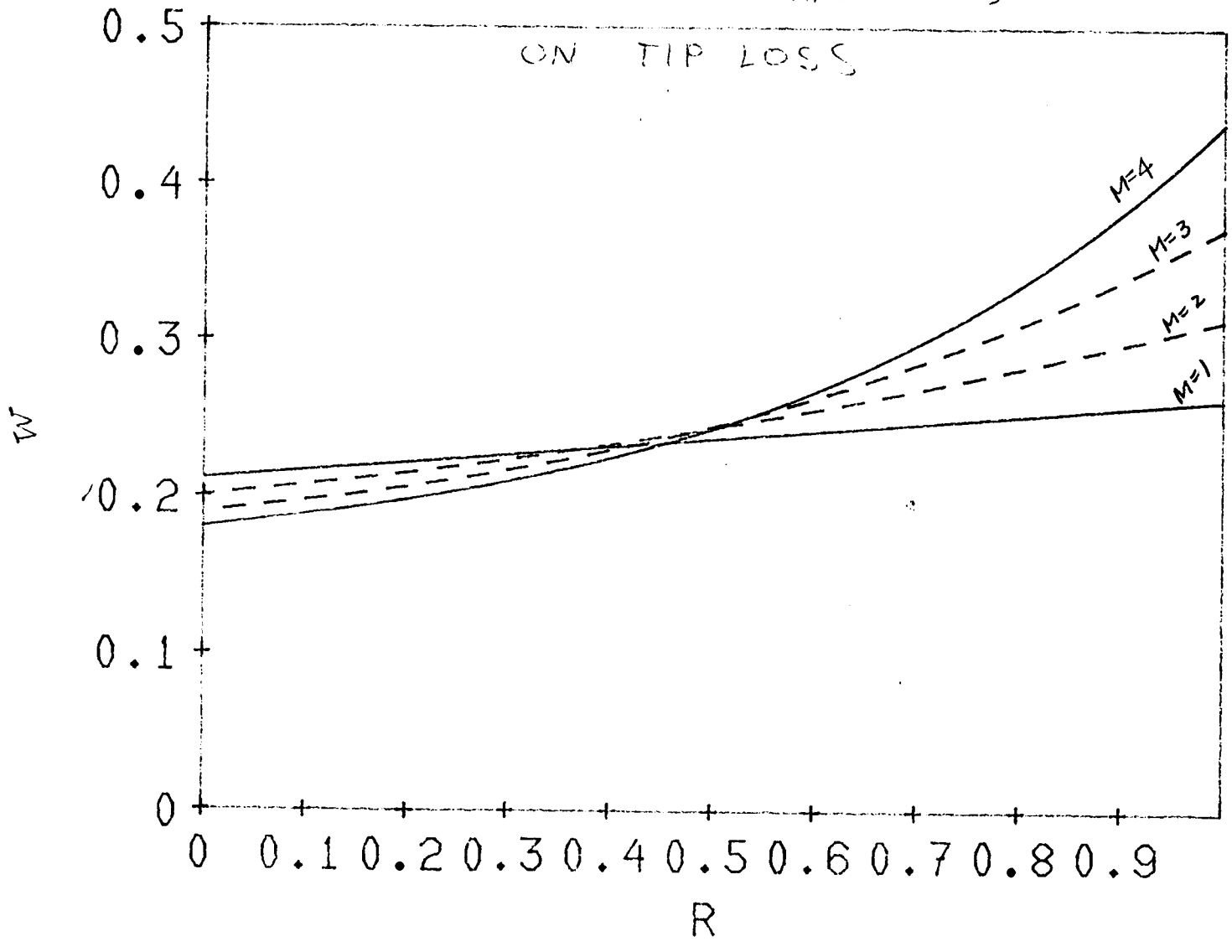

periodic coefficient, $\beta = \overset{*}{\beta} = 0$, $\theta = 1$, $\sigma a = 0.2$

FIG. 5 B EFFECT OF S ON TIP LOSS

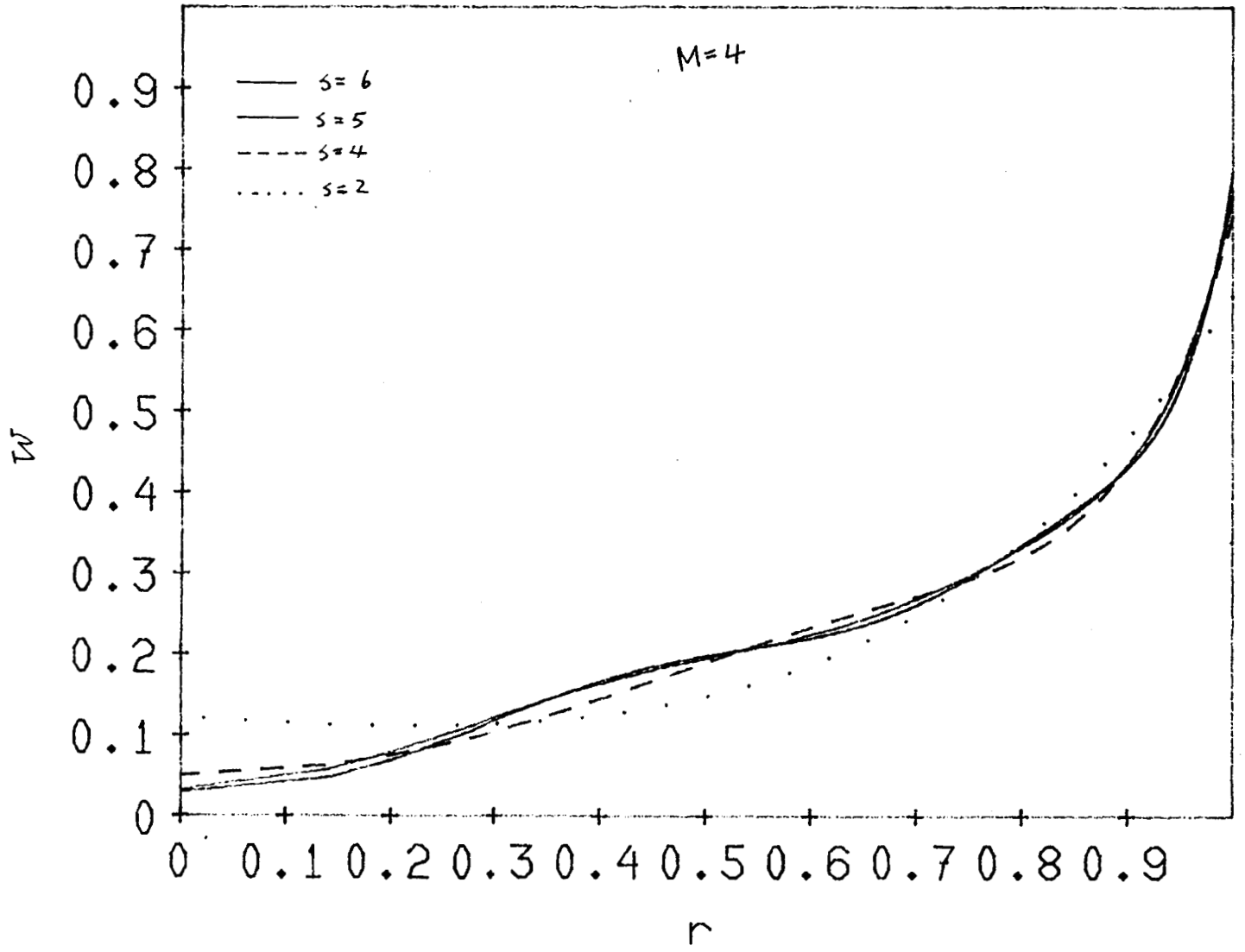

Δ - P_n^m

o - $\frac{1}{\nu} P_n^m$

FIG. 6a

THE INDUCED VELOCITY DISTRIBUTION (M=0)

FIRST MODE

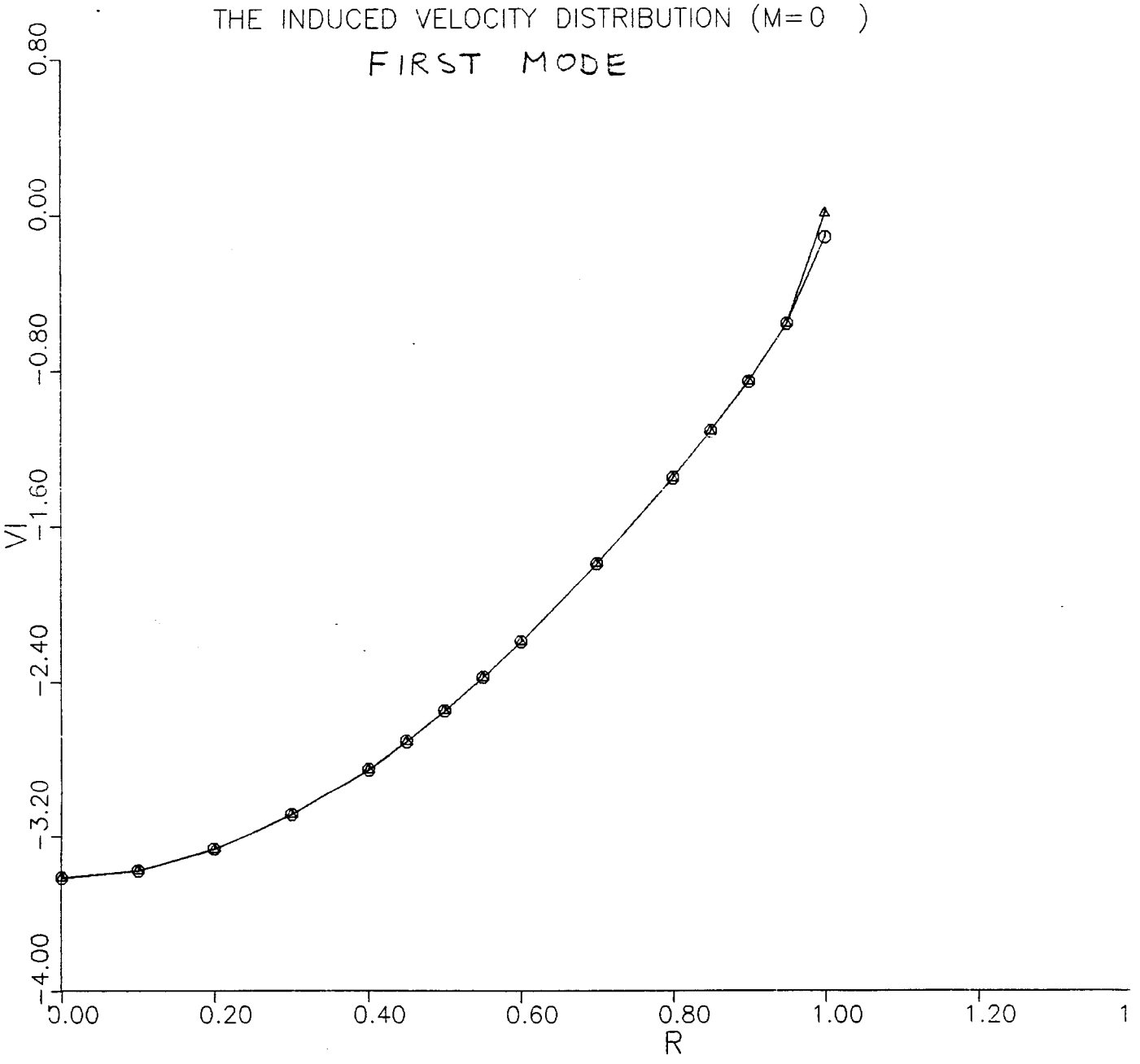

Fig. 6b

THE INDUCED VELOCITY DISTRIBUTION (M=1)

FIRST MODE

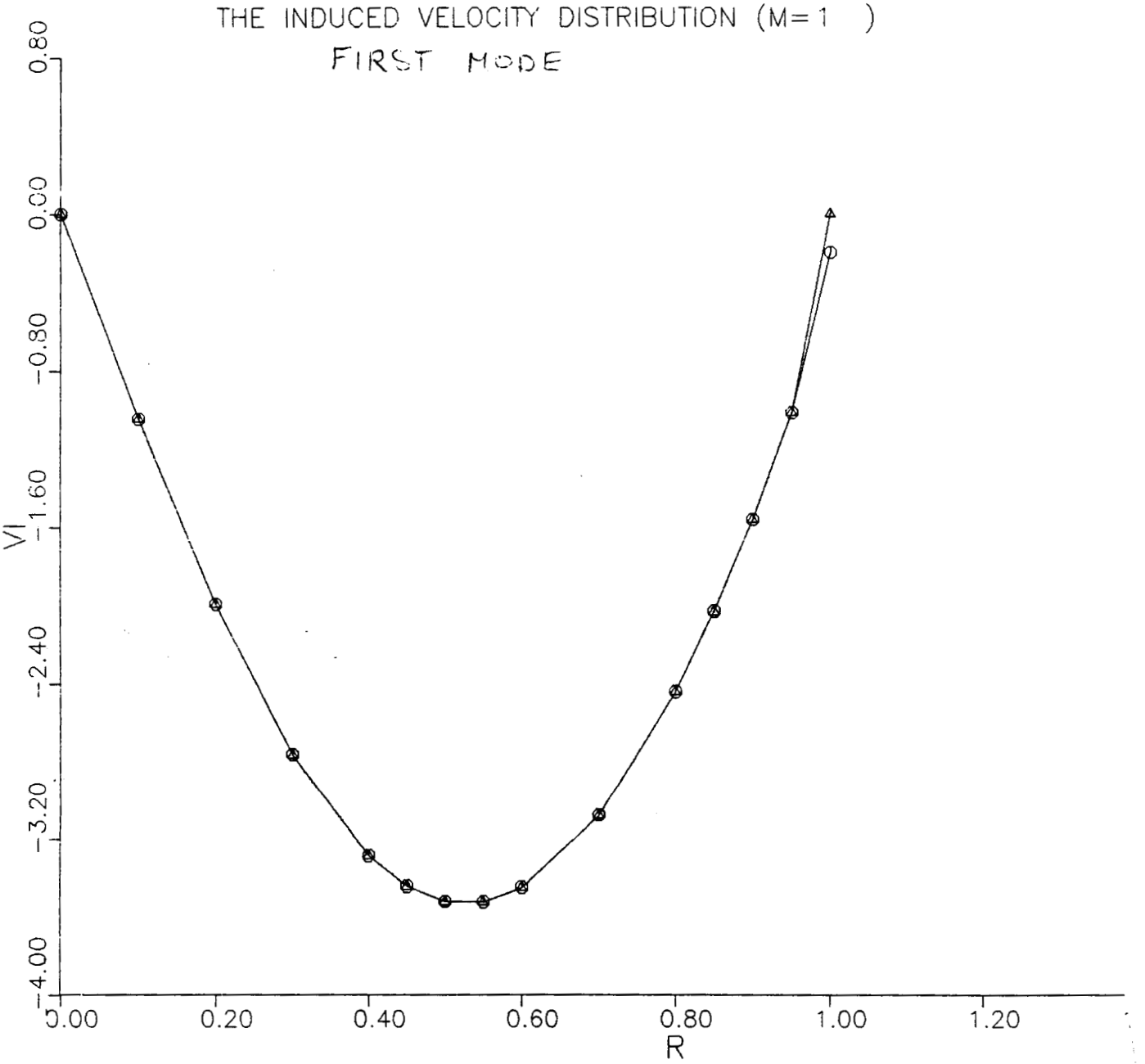

FIG. 6C

THE INDUCED VELOCITY DISTRIBUTION (M=2 ,MODE 1)

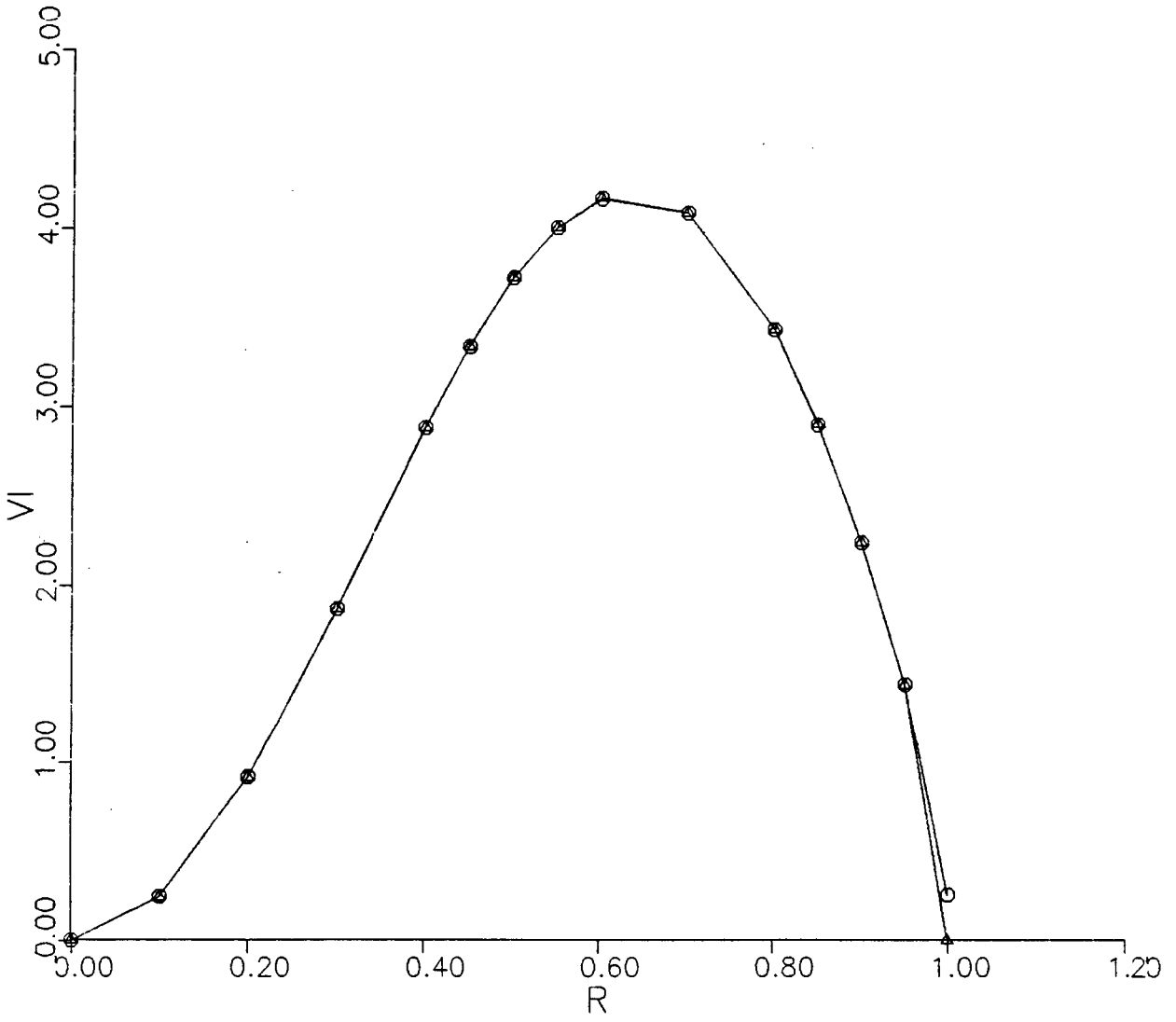

FIG. 6d

THE INDUCED VELOCITY DISTRIBUTION (M=3 ,MODE 1)

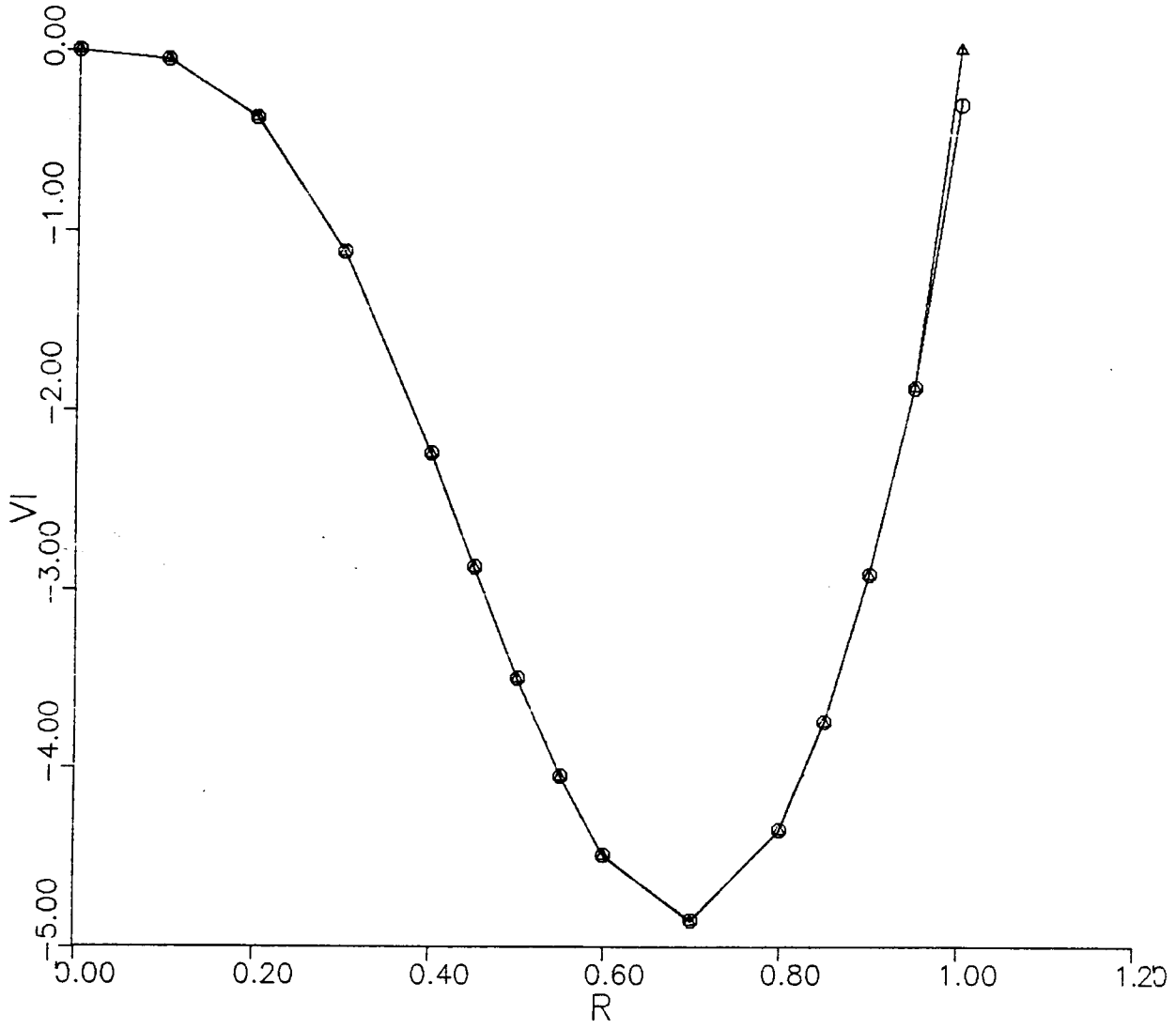

Fig. 6e

THE INDUCED VELOCITY DISTRIBUTION (M=4 ,MODE 1)

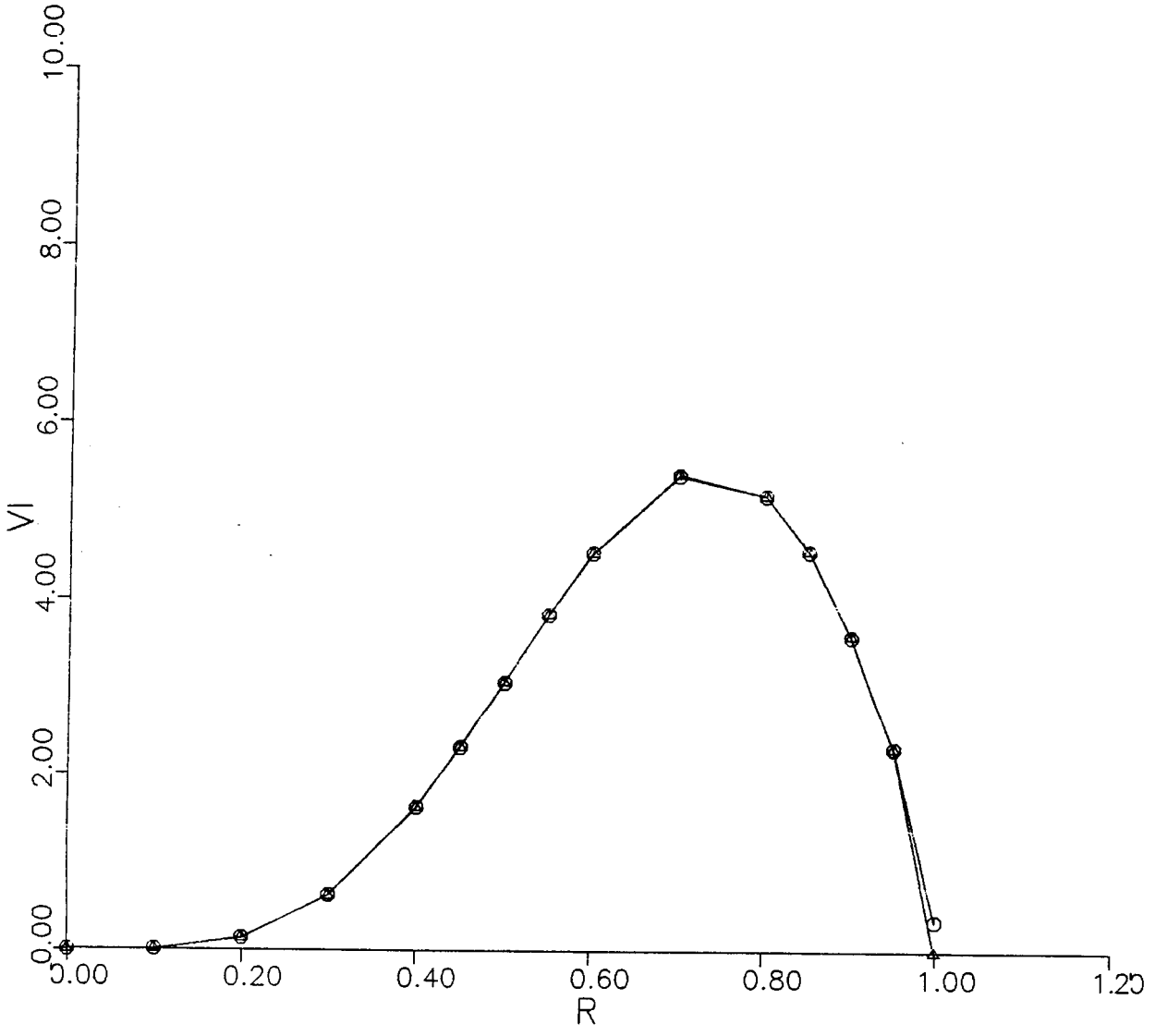

Fig. 7a

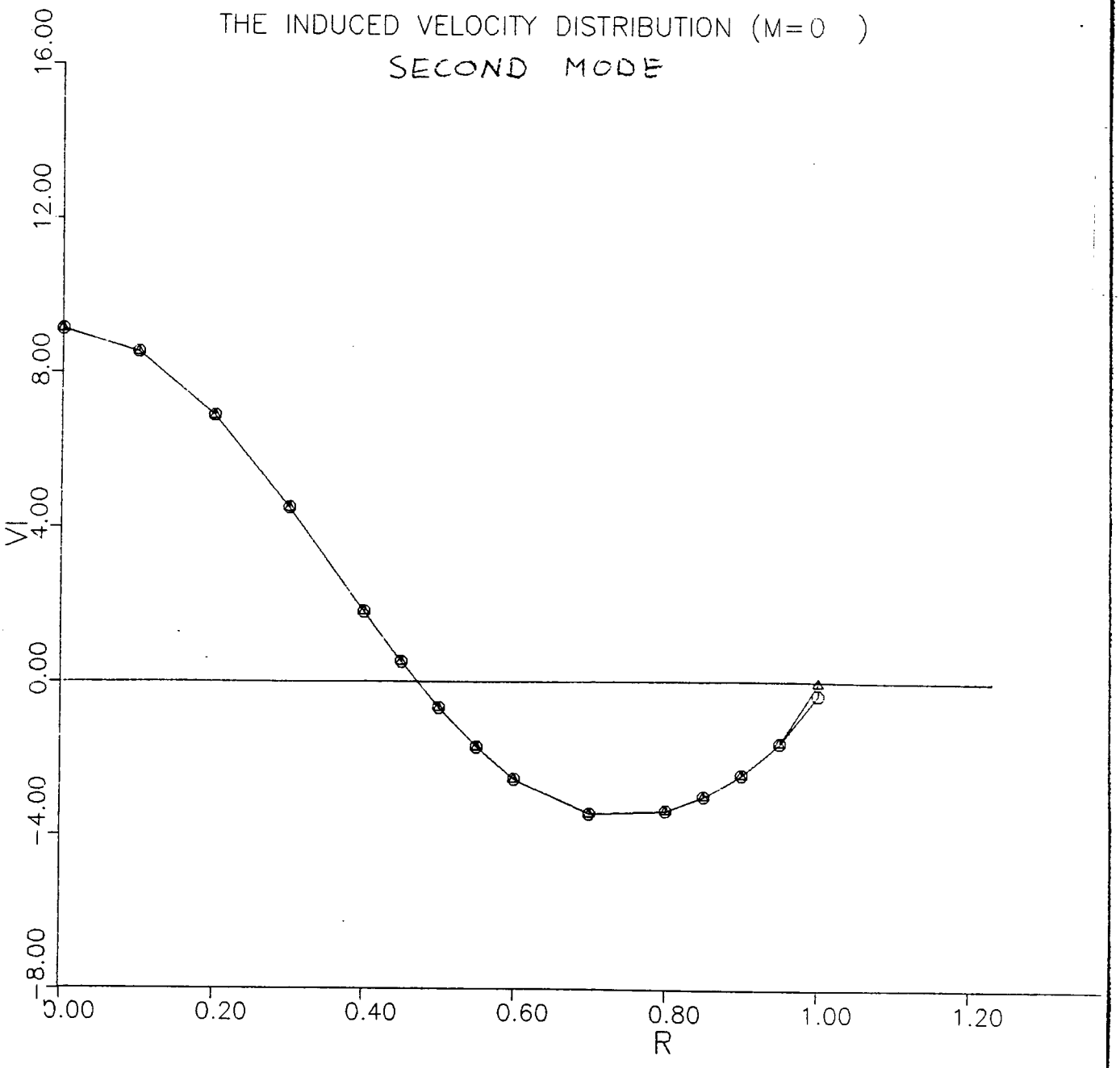
THE INDUCED VELOCITY DISTRIBUTION (M=0)
SECOND MODE
16.00
12.00
8.00
4.00
0.00
-4.00
-8.00
VI
0.00
0.20
0.40
0.60
0.80
1.00
1.20
R

2nd

FIG 75

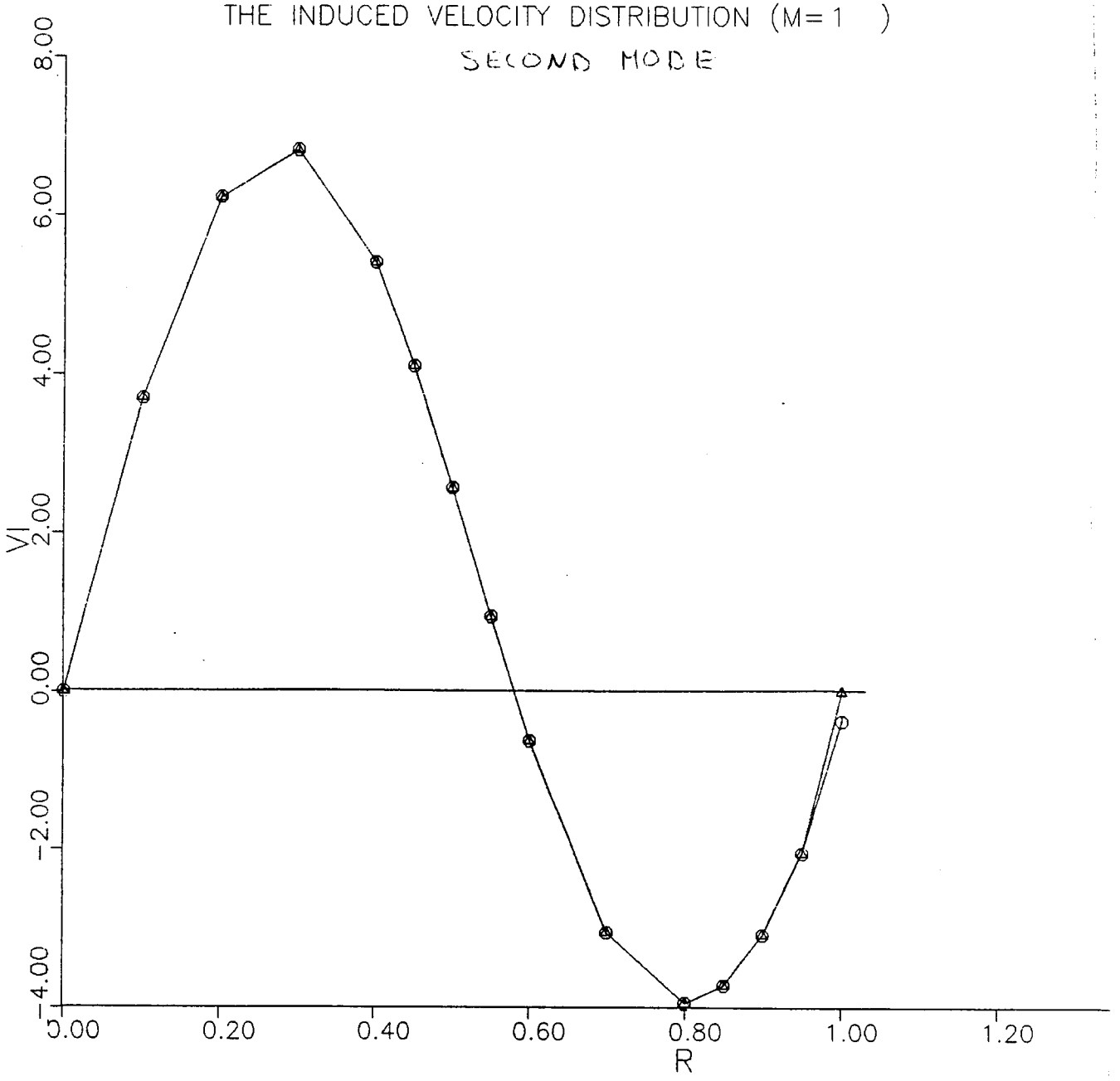
THE INDUCED VELOCITY DISTRIBUTION (M=1)
SECOND MODE
8.00
6.00
4.00
2.00
0.00
-2.00
-4.00
VI
0.00
0.20
0.40
0.60
0.80
1.00
1.20
R

FIG. 7c

THE INDUCED VELOCITY DISTRIBUTION (M=2 ,MODE 2)

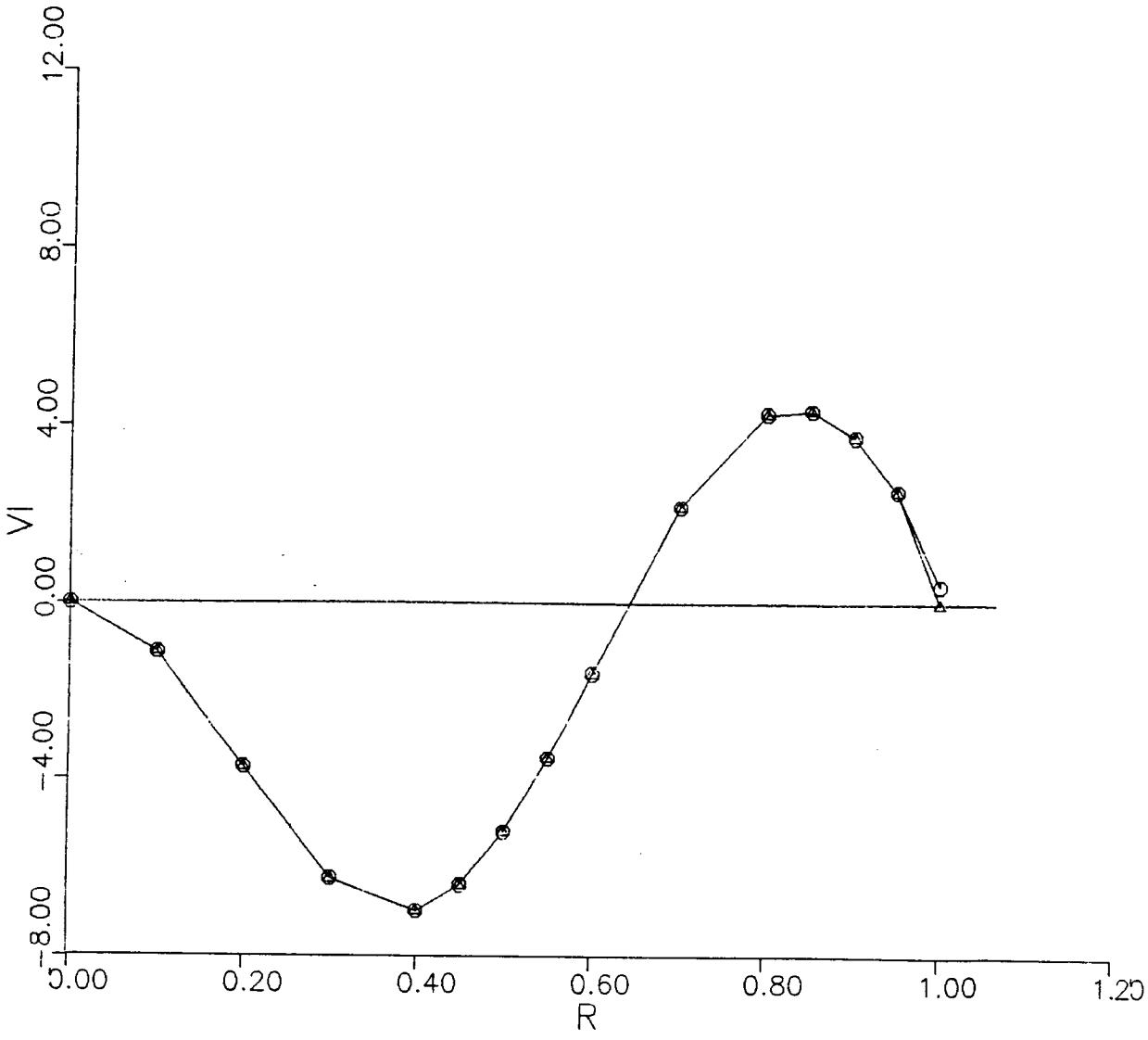

FIG. 7d

THE INDUCED VELOCITY DISTRIBUTION (M=3 ,MODE 2)

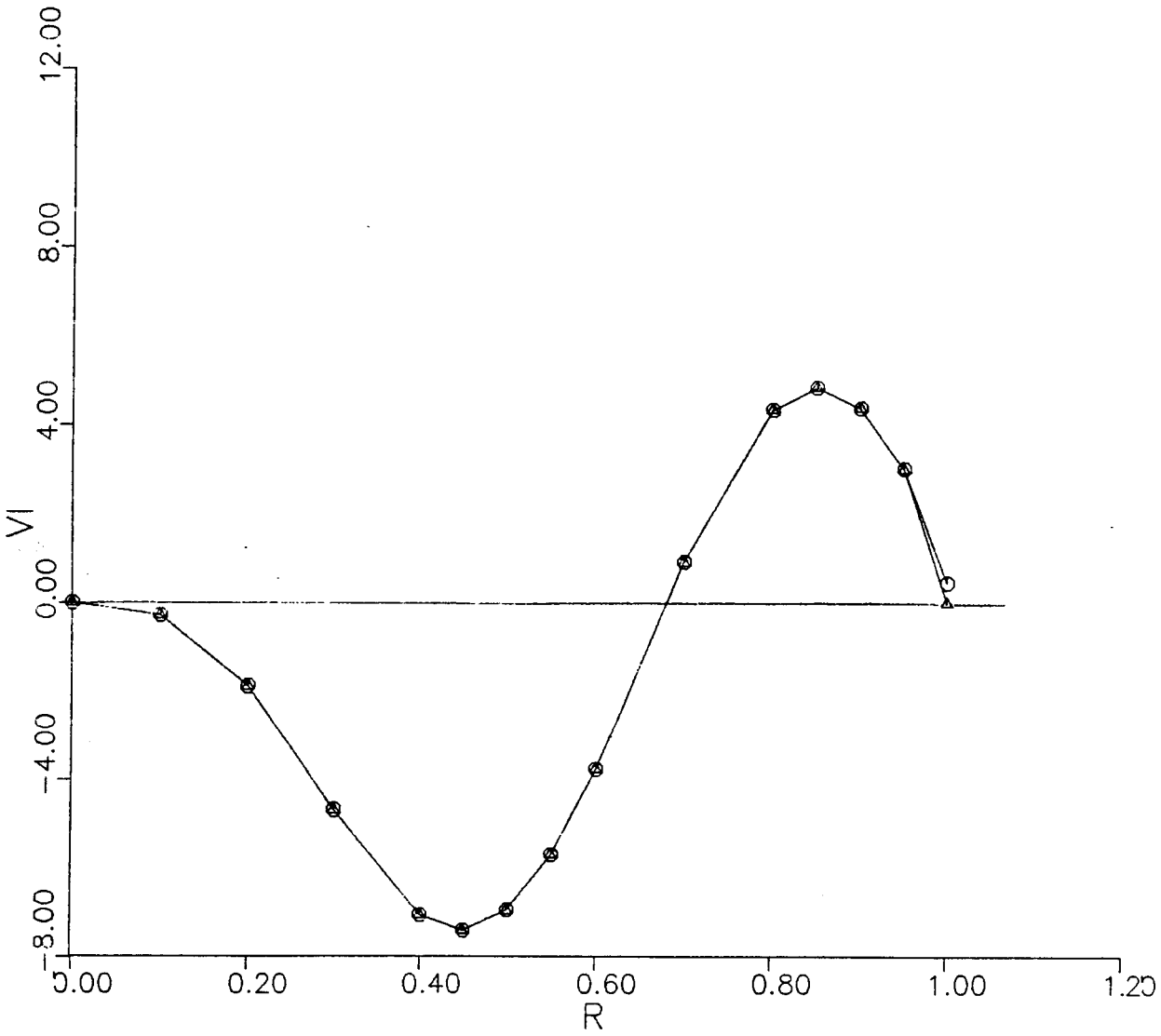

FIG. 7e

THE INDUCED VELOCITY DISTRIBUTION (M=4 ,MODE 2)